ChemComm

COMMUNICATION

View Article Online
View Journal

Cite this: DOI: 10.1039/c9cc07968h

Received 11th October 2019,
Accepted 2nd December 2019

DOI: 10.1039/c9cc07968h

rsc.li/chemcomm

A facile strategy to realize a single/double photon excitation-dependent photosensitizer for imaging-guided phototherapy against HeLa cancer cells at separate irradiation channels†

Lin Kong, *[a] Ze Huang,[a] Shuai-Shuai Zhang,[a] Jian Song,[b] Yu-Yang Zhang,[a] Xiang-Yang Bai,[a] Jia-Xiang Yang *[a] and Lin Li *[c]

A novel difluoroboron fluorophore with an electron donor–acceptor conjugated structure was synthesized with 26.5% fluorescence quantum yield, 18 035 GM two-photon absorbing cross-section, and undetectable two-photon fluorescence, resulting in 25% $^1O_2$ quantum yield. The unique optical behavior of CNFBBN enabled one-photon fluorescence imaging and two-photon phototherapy against HeLa cancer cells, irradiated at separate wavelengths.

In recent years, phototherapy against living cancer cells and/or malignant tumors has shown a significant upward trend due to some unique advantages, such as short treatment time (a few minutes), reliable therapeutic outcome, and no-resistance.[1] Commonly used methods for phototherapy include photothermal and photodynamic therapy. In general, phototherapy agents require strong energy transfer or dissipation, such as photothermal conversion or reactive oxygen species (ROS, including singlet oxygen $^1O_2$) generation. To achieve this, strong absorption and low fluorescence are required.[2] In the latest medical field, fluorescence mediated phototherapy can assist in deciding the irradiation region and drug/light doses, to monitor the clinical effect and decide the best timing/intensity of irradiation,[3] which would require high fluorescence quantum yield (QY) of the agent.[4] Considering the two opposite trends, phototherapeutic efficiency and fluorescence imaging effect are trade-off processes.

To achieve both a high therapeutic efficiency and excellent imaging effect, many phototherapeutic agents are combined with fluorescent materials.[5] In 2017, Yang exploited the photothermic effect of Ag_2S nanodots to kill 4T1 cells, and simultaneously used the high QY of a fluorescent dye Cy7.5 to monitor drug targeting and therapeutic procedures.[6] Such composite materials may require large doses and involve security risks.[7] Then, scientists turned to the search for a single agent that can possess both fluorescence properties and phototherapeutic characteristics.[8] In 2014, Liu *et al.* developed a wavelength-dependent multifunctional photosensitizer, which exhibited a strong/weak or strong/no emitting signal at different wavelength channels.[9] Such materials should emit fluorescence for imaging at a particular excitation wavelength and radiate phototherapeutic beams at a different wavelength. To construct such agents, electron-donor–acceptor (D–A) conjugated structures with two-photon absorbing (TPA) character can be applied for architecting both efficient two-photon photo-theranostic function and one-photon fluorescence emission.[10] For most TPA materials, the optimal two-photon excitation wavelength is located in the near-infrared region, and the value is twice that of the one-photon excitation wavelength.[11] So, imaging and therapy can be easily regulated at separated irradiation channels. The search for photosensitizers with bright one-photon fluorescence (OPEF) and strong TPA character is the aim of this strategy.

The high two-photon photothermal conversion or $^1O_2$ generation can be achieved through intramolecular charge transfer (ICT), which is a reliable method for quenching two-photon excited fluorescence (TPEF) by introducing a strong electron-withdrawing/donating unit into the molecule.[12] Recently, Tang proposed that the advantages of dark twisted ICT originating from electron-donating/accepting structures can be used to achieve molecular motion in aggregates and improve photothermal conversion[13] or produce $^1O_2$ with high efficiency.[14] However, an effective energy transfer or dissipation is difficult to achieve in a single organic dye with high OPEF QY under TP irradiation, which necessitates developing a simple strategy for establishing a structure–performance correlation of such agents.

[a] College of Chemistry and Chemical Engineering, Anhui Province Key Laboratory of Chemistry for Inorganic/Organic Hybrid Functionalized Materials, Anhui University, Hefei 230601, P. R. China. E-mail: kong_lin2009@126.com, jxyang@ahu.edu.cn

[b] College of Physics and Materials Science, Henan Normal University, Xinxiang 453007, China

[c] Laboratory of Flexible Electronics (KLOFE) & Institute of Advanced Materials (IAM), National Jiangsu Synergistic Innovation Center for Advanced Materials (SICAM), Nanjing Tech University, Nanjing 211816, P. R. China. E-mail: iamlli@njtech.edu.cn

† Electronic supplementary information (ESI) available: Experimental details: preparation and characterization of CNFBBN, linear/nonlinear optical properties, detailed biological tests, cellular ROS detection, and quantum calculation. See DOI: 10.1039/c9cc07968h

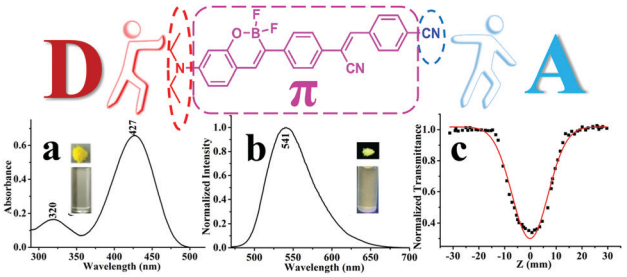

Fig. 1 Top: The structure of CNFBBN and the schematic diagram of electron-withdrawing/donating strength within it; (a) absorption spectrum in DMSO solution and (b) fluorescence spectrum in the solid state excited at 430 nm (inset: photographs under room-light and a 365 nm lamp). (c) Open *Z*-scan experimental result in DMSO solution under 840 nm irradiation. Solid lines show fitting to experimental data.

In this study, a novel boron-Schiff base complex was designed and synthesized (ESI† parts S2–S4). A cyano unit (as a strong electron-withdrawing group) was linked with the electron donor *N*,*N*-diethylaminoaniline unit to form a D–A type compound, abbreviated as CNFBBN (top of Fig. 1).

The organo-boron coordination and a known aggregation induced enhanced emission (AIEE) unit (4,4′-dicyanophenylethynylene) were introduced to achieve high OPEF QY both in solution and solid-state (26.5%). CNFBBN also exhibited a high molar absorption coefficient (ε, 3.75×10^5 L cm^{-1} mol^{-1})[15] and 18 035 GM (1 GM = 10^{-50} cm^4 s per photon) TPA cross-section (δ_{TPA}) in DMSO solution. But its TPEF signal was undetectable due to the strong ICT process. So, most of the absorbed energy was transferred to adjacent oxygen through an intersystem crossing (ISC) process, which led to 25% $^1O_2$ QY. Upon TP irradiation, 70% of HeLa cancer cells were killed, and the OPEF signal can be used to monitor the cell ablation process. The results showed that this type of difluoride boron fluorophore could simultaneously integrate OPEF imaging mediated TP phototherapy treatment against living HeLa cells at high brightness with significantly high cancer cell killing efficiency.

CNFBBN exhibited two UV-vis absorption bands in DMSO solution (Fig. 1a). One was located at 320 nm arising from the π–π* transition of the whole conjugated structure. The other was focused at 427 nm contributing to the ICT band that was promoted from the strong D–A strength. The molar absorption coefficient (ε) was as high as 3.75×10^5 L cm^{-1} mol^{-1}. Upon illuminating with a 365 nm ultraviolet lamp, CNFBBN radiated yellow-colored emission (541 nm, Fig. 1b) with 26.5% QY in the solid-state (Fig. S3, ESI†). The fluorescence of CNFBBN in DMSO solution displayed a band at 558 nm with 0.9% QY (Table S1 and Fig. S2, ESI†) and 0.03 ns fluorescence lifetime (Table S2 and Fig. S4, ESI†) when it was excited at 430 nm. The corresponding radiative transition rate K_r was calculated to be 3.33×10^{10} s^{-1}. The non-radiative transition rate K_{nr} was 3.67×10^8 s^{-1}. CNFBBN displayed a strong ICT process as its QY in polar solvent (DMSO here) was much lower than that in non-polar solvent (*i.e.* 0.78 in Bz), which might cause energy loss *via* a fast non-radiative transition from the excited state in polar solvents, and then led to a short fluorescence lifetime.[13] Its fast non-radiative transition could be effectively used for bio-applications in this study.

Moreover, CNFBBN exhibited a decrease in transmittance under the open-*Z*-scan experiment, which revealed a positive nonlinear optical effect and TPA character (Fig. 1c). The minimum transmittance at $Z = 0$ was 48.1% with a related TPA coefficient β value of 0.04699 cm GW^{-1} (eqn (S1), ESI†) and a δ_{TPA} value of 18 035 GM (eqn (S2), ESI†). The related active TPA cross-section $\phi\delta$ was as high as 162 GM, suggesting that CNFBBN could be used as a suitable TP agent for biological applications. However, under similar circumstances, the TPEF signal was not captured. The excellent TPA performance and undetectable TPEF signal indicated potential two-photon induced energy transfer or dissipation.

The photodynamic therapeutic effect of CNFBBN is determined by ROS and $^1O_2$ generation. The auto-oxidation of CNFBBN in aqueous suspension was measured and compared against chlorin e6 (Ce6). CNFBBN released 2.13-fold higher levels of ROS than Ce6 during irradiation (Fig. 2a and Fig. S6, ESI†), which revealed that CNFBBN was indeed an excellent ROS producing agent. Furthermore, 25% $^1O_2$ QY of CNFBBN was captured by comparing to Rose Bengal (Fig. 2b and Fig. S7, ESI†). Based on these results, we speculated that ROS and $^1O_2$ were produced from the strong D–A strength of CNFBBN and the corresponding small energy level difference between a singlet and triplet (see below for details), which effectively transferred the absorbed energy to the surrounding oxygen to generate ROS especially $^1O_2$ for killing cancer cells in photo-therapeutic treatment.[16]

To better understand the photophysical properties at different irradiation channels, especially the decreased emission and easy singlet–triplet conversion effect under two-photon excitation, quantum chemical calculations using time-dependent density functional theory (TD-DFT) were employed. The excited-state potential energy surfaces of CNFBBN were investigated to explain the decrease in the emission mechanism.[17] The difference in potential energy was relatively small (10–12 kJ mol^{-1}) compared to the changeable rotor angle at two main spots of the molecule, one was around the coordination center of the boron atom (Fig. 3a) and the other was in the cyanostilbene unit (Fig. 3b). These two points exhibited a small difference in potential energy, *i.e.* a small barrier to rotation.[18] The results suggested that the excited CNFBBN molecule can relax to its minimum on the S_1 potential energy surface upon rotation, which primarily relaxed through the non-radiative process and was responsible for the quenching of the emission.[19] The experimental data verified this

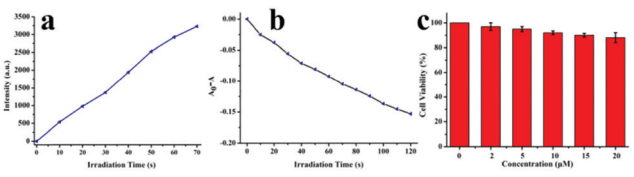

Fig. 2 (a) Time-dependent fluorescence intensity of DCF in the presence of CNFBBN during 70 second irradiation. (b) Time-dependent absorbance evolution of ABDA in the presence of CNFBBN during 120 s irradiation. (c) Cell viability as measured by an MTT assay at different concentrations. Data are shown as mean ± SD, $n = 3$.

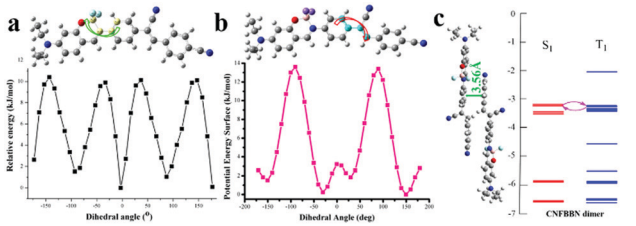

Fig. 3 (a and b) Excited (bottom) B3LYP TD-DFT state energies of CNFBBN as a function of dihedral angle at desired spots (the data were compared with that in a natural state with the rotor angle being 0°). The excited state is based on the TDDFT-computed oscillator strength (f_{osc}) for an electric-dipole-allowed transition between the ground and excited states. Rotation in the excited state located at the specific spots shown in the top image. (c) Calculated selected molecular orbital energy diagrams for the singlet ground (S_0), first singlet state (S_1) and first triplet state (T_1) of the CNFBBN dimer.

calculated result as K_{nr} of CNFBBN was 110-fold slower than K_r (described above).

Except for the molecular rotation, the TPA/TPEF performance is another important factor in the quenched emission of CNFBBN. The maximum calculated δ_{TPA} value of CNFBBN was 2026 GM using eqn (S3) (ESI†). The predicted TPA wavelength blue-shifted when the temperature was increased from 200 K to 400 K, while the TPEF band red-shifted with increasing temperature (Fig. S13, ESI†). A similar experimental phenomenon was observed for OPEF as shown in Fig. S14 (ESI†), suggesting the accuracy of the calculation. As the optimized experimental TPA wavelength was 840 nm in DMSO solution, and the strongest emission signal was located around 558 nm, when CNFBBN was irradiated under a two-photon laser which might lead to an increase in temperature to some extent at the localized irradiation spot, the blue-shifted TPA band partly overlapped with the red-shifted emission band (possibly existed), which caused re-absorption phenomena.[20] In this situation, excitation by a TP laser and the related re-absorption hindered the radiation channel of CNFBBN, resulting in diminished TPEF.[21] The raised proportion of non-radiative transition and the blocked radiating channel were the main reasons for the undetectable TPEF signal of CNFBBN.

Moreover, a small energy gap between the singlet and triplet excited states might be beneficial for ISC and further produce reactive oxygen species. To accurately reflect the behavior of CNFBBN in biological systems, two molecules forming a dimer were built as calculating models to simulate a possible aggregation behavior of CNFBBN in aqueous medium.[22] Molecular orbitals' energy splitting was observed in both S and T states (Fig. 3c). An obvious S–T overlap was clearly captured, attributing to the energy increase in the nearby oxygen molecules, which was useful for killing cancer cells.

CNFBBN had low dark cytotoxicity on cancer HeLa cells. The cell survival at different concentrations was tested through the MTT assay. As shown in Fig. 2c, the cell viability was higher than 90% until the concentration of CNFBBN was 10 μmol L^{-1}, and still exhibited 88% survival rate when the concentration was up to 20 μmol L^{-1}.

Then, HeLa cells were incubated with 10 μmol L^{-1} CNFBBN for 30 min. CNFBBN penetrated the cell cytosol *via* energy-dependent endocytosis (Fig. S10a and b, ESI†) within a short incubation period, which suggested an endosomal- and/or lysosomal-like interaction. The TPEF signal of CNFBBN was not captured in HeLa cells (Fig. 4a-2). The co-localization experiment (Fig. 4b) suggested that CNFBBN was associated with the lipophilic region and bonded at the endoplasmic reticulum (ER) part of HeLa cells with Pearson's coefficient R_r being 0.92, possibly because that the ER is a membrane-rich organelle with high hydrophobicity and CNFBBN is a lipophilic molecule. The fluorescence signal observed from Fig. 4b-1 was considered as the intrinsic emission of CNFBBN as the weak alkaline environment of ER in HeLa cells[23] may not significantly change it as shown in the ESI,† Fig. S15.

Furthermore, the potential use of CNFBBN as a TPA agent in two-photon phototherapy was evaluated *in vitro*. Firstly, the two-photon photocytotoxicity of CNFBBN was tested. The cell viability did not change significantly under non-irradiation in Fig. 2c as discussed above. However, the cell viability sharply decreased to 30% when CNFBBN co-incubated cells were treated with 840 nm irradiation for 10 min (Fig. 5c). Two other control experiments were also performed. When one-photon laser irradiated CNFBBN was co-incubated with HeLa cells for 10 min, 76% survived (Fig. S9, ESI†). Only two-photon laser irradiation for 10 min can bring about 19% cell damage as shown in Fig. S9 (ESI†). The phenomenon revealed that combining CNFBBN with TP irradiation led to high phototoxicity.

Moreover, the therapeutic effect on HeLa cells was clearly observed from the bright field of one-photon fluorescence microscopy (OPFM) imaging, especially the red-circled parts in Fig. 5a. The OPFM images in Fig. 5b showed that aggregation phenomena occurred during the irradiation procedure, which was beneficial for the accelerated destruction of HeLa cells after 3 min irradiation. As discussed previously, CNFBBN was mostly located at the ER part of HeLa cells. When CNFBBN incubated cells were irradiated, an effective $^1O_2$ release occurred and the integrity of the cytoplasm was destroyed, causing two-photon phototherapy (Fig. 5a). When the illumination time was longer

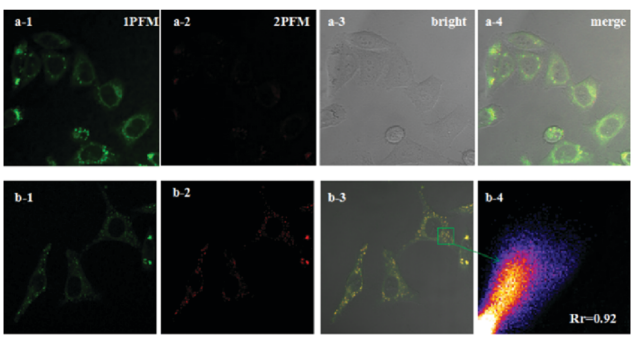

Fig. 4 (a1–a4) Fluorescence images of living HeLa cells incubated with 10 μmol L^{-1} CNFBBN for 30 min with one-photon (405 nm) excitation (a1) and two-photon (840 nm) excitation (a2). (b1–b4) Confocal co-localization studies of CNFBBN upon OPFM of CNFBBN and ER-tracker red at the same dose of 10 μmol L^{-1}, (b1) OPFM of CNFBBN (λ_{ex} = 405 nm), (b2) OPFM of ER-tracker red (λ_{ex} = 545 nm), (b3) merging of (b1) and (b2), and (b4) co-localization.

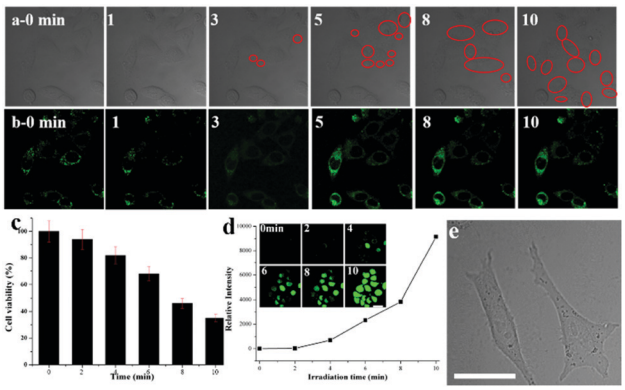

Fig. 5 (a and b) Confocal images of bright field and confocal OPFM images of CNFBBN stained HeLa cells during TP treatments at different irradiation times. The red circles showed the cellular apoptosis process. The excited wavelength for two-photons was 840 nm and 405 nm for one-photon. (c) Cell viability as measured by an MTT assay at different irradiation times. Data are shown as mean ± SD, n = 3. (d) Relative fluorescence intensity of DCFH-DA in CNFBBN-DCFH DA-HeLa cells at 840 nm for 0, 2, 4, 6, 8, and 10 min; and (e) bright image of HeLa cells treated under irradiation for 10 min without CNFBBN co-incubation. The dose was kept at 10 μmol L^{-1}.

than 8 min, the destruction of the cell membrane began to occur. In 10 min, most of the cells under the view field were ablated. The relative fluorescence intensity of $^1O_2$ trapper DCFH-DA increased ~2000 fold during this process (Fig. 5d), which clearly suggested that the $^1O_2$ generation was effective in CNFBBN incubated HeLa cells during TP irradiation. A control test was also performed; however, almost no treatment effect was observed in HeLa cells that were treated under irradiation but without CNFBBN co-culture, as shown in Fig. 5e.

In summary, a D–A structured fluoroboron (CNFBBN) has been designed and synthesized, and possesses low dark toxicity towards HeLa cells, high fluorescence QY and excellent TPA character but an undetectable TPEF signal. Thus, CNFBBN exhibits excellent $^1O_2$ production under TP irradiation, which makes it act as a promising photosensitizer for two-photon phototherapy with simultaneous imaging modality at separated irradiation channels. Therefore, the development of this D–A type fluoroboron-based one/two photon excitation-dependent photosensitizer may be a reasonable approach for promoting the cell imaging-guided phototherapy, a clinically acceptable therapeutic method at separated irradiation channels.

This work was supported by the Educational Commission of Anhui Province of China (KJ2019A0012), the NSFC (No. 51673001 and 81672508).

Conflicts of interest

There are no conflicts to declare.

References

1 W. Sang, Z. Zhang, Y. L. Dai and X. Y. Chen, *Chem. Soc. Rev.*, 2019, **48**, 3771–3810.
2 J. J. Hu, Y. J. Cheng and X. Z. Zhang, *Nanoscale*, 2018, **10**, 22657–22672.
3 Y. G. Y. G. Shi, M. Y. Liu, F. J. Deng, G. J. Zeng, Q. Wan, X. Y. Zhang and Y. Wei, *J. Mater. Chem. B*, 2017, **5**, 194–206.
4 Q. A. Best, A. E. Johnson, B. Prasai, A. Rouillere and R. L. McCarley, *ACS Chem. Biol.*, 2016, **11**, 231–240; W. S. Shin, M. G. Lee, P. Verwilst, J. H. Lee, S. G. Chi and J. S. Kim, *Chem. Sci.*, 2016, **7**, 6050–6059.
5 R. T. R. T. K. Kwok, C. W. T. Leung, J. W. Y. Lam and B. Z. Tang, *Chem. Soc. Rev.*, 2015, **44**, 4228–4238.
6 T. Yang, Y. A. Tang, L. Liu, X. Y. Lv, Q. L. Wang, H. T. Ke, Y. B. Deng, H. Yang, X. L. Yang, G. Liu, Y. L. Zhao and H. B. Chen, *ACS Nano*, 2017, **11**, 1848–1857.
7 P. Huang, P. F. Rong, A. Jin, X. F. Yan, M. G. Zhang, J. Lin, H. Hu, Z. Wang, X. Y. Yue, W. W. Li, G. Niu, W. B. Zeng, W. Wang, K. C. Zhou and X. Y. Chen, *Adv. Mater.*, 2014, **26**, 6401–6408.
8 M. H. M. H. Lan, L. Guo, S. J. Zhao, Z. Y. Zhang, Q. Y. Jia, L. Yan, J. Xia, H. Y. Zhang, P. F. Wang and W. J. Zhang, *Adv. Ther.*, 2018, **1**, 1800077; J. C. Li and K. Y. Pu, *Chem. Soc. Rev.*, 2019, **48**, 38–71.
9 Q. Chen, C. Wang, Z. X. Zhan, W. W. He, Z. P. Cheng, Y. Y. Li and Z. Liu, *Biomaterials*, 2014, **35**, 8206–8214.
10 Y. J. Y. J. Liu, P. Bhattarai, Z. F. Dai and X. Y. Chen, *Chem. Soc. Rev.*, 2019, **48**, 2053–2108; C. H. Heo, A. R. Sarkar, S. H. Baik, T. S. Jung, J. J. Kim, H. Kang, I. M. Jung and H. M. Kim, *Chem. Sci.*, 2016, **7**, 4600–4606.
11 M. Pawlicki, H. A. Collins, R. G. Denning and H. L. Anderson, *Angew. Chem., Int. Ed.*, 2009, **48**, 3244–3266; A. Khadria, Y. De Coene, P. Gawel, C. Roche, K. Clays and H. L. Anderson, *Org. Biomol. Chem.*, 2017, **15**, 947–956.
12 Y. Lyu, Y. Fang, Q. Miao, X. Zhen, D. Ding and K. Pu, *ACS Nano*, 2016, **10**, 4472–4481.
13 S. J. Liu, X. Zhou, H. K. Zhang, H. L. Ou, J. W. Y. Lam, Y. Liu, L. Q. Shi, D. Ding and B. Z. Tang, *J. Am. Chem. Soc.*, 2019, **141**, 5359–5368.
14 Z. Zheng, T. F. Zhang, H. X. Liu, Y. C. Chen, R. T. K. Kwok, C. Ma, P. F. Zhang, H. H. Y. Sung, I. D. Williams, J. W. Y. Lam, K. S. Wong and B. Z. Tang, *ACS Nano*, 2018, **12**, 8145–8159.
15 J. Z. J. Z. Zhao, K. J. Xu, W. B. Yang, Z. J. Wang and F. F. Zhong, *Chem. Soc. Rev.*, 2015, **44**, 8904–8939; T. Zhang, C. Ma, T. T. Sun and Z. G. Xie, *Coord. Chem. Rev.*, 2019, **390**, 76–85.
16 W. B. Wu, D. Mao, S. D. Xu, Kenry, F. Hu, X. Q. Li, D. L. Kong and B. Liu, *Chem*, 2018, **4**, 1937–1951.
17 Q. H. Liu, X. Y. Zhou, L. S. Zhou, Y. L. Zhang, X. Luo, H. Guo and B. Jiang, *J. Phys. Chem. C*, 2018, **122**, 1761–1769.
18 M. P. Metz, K. Szalewicz, J. Sarka, R. Tóbiás, A. G. Császár and E. Mátyus, *Phys. Chem. Chem. Phys.*, 2019, **21**, 13504–13525.
19 C. Qu, Q. Yu and J. M. Bowman, *Annu. Rev. Phys. Chem.*, 2018, **69**, 151–175.
20 D. C. Hong, J. Li, S. S. Wan, I. G. Scheblykin and Y. X. Tian, *J. Phys. Chem. C*, 2019, **123**, 12521–12526.
21 Y. P. Ma, J. Sun and X. B. Luo, *J. Lumin.*, 2019, **209**, 109–115.
22 X. X. Sun, X. J. Wang, X. Y. Li, J. Ge, Q. Zhang, J. Jiang and J. Q. Zhang, *Macromol. Rapid Commun.*, 2015, **36**, 298–303.
23 B. L. Dong, W. H. Song, Y. Lu, X. Q. Kong, A. H. Mehmood and W. Y. Lin, *Chem. Commun.*, 2019, **55**, 10776–10779.

